Polymer 49 (2008) 4852–4860

Contents lists available at ScienceDirect

Polymer

journal homepage: www.elsevier.com/locate/polymer

Thermal properties and surface energy characteristics of interpenetrating polyacrylate and polybenzoxazine networks

Chu-Hua Lu [a], Yi-Che Su [b], Chih-Feng Wang [c], Chih-Feng Huang [a], Yuung-Ching Sheen [a,b], Feng-Chih Chang [a,*]

[a] Institute of Applied Chemistry, National Chiao Tung University, 30010 Hsinchu, Taiwan
[b] Material and Chemical Research Laboratories, Industrial Technology Research Institute, 30050 Hsinchu, Taiwan
[c] Department of Chemical and Materials Engineering, I-Shou University, 84008 Kaohsiung, Taiwan

ARTICLE INFO

Article history:
Received 15 May 2008
Received in revised form 29 August 2008
Accepted 2 September 2008
Available online 12 September 2008

Keywords:
Interpenetrating polymer networks
Polybenzoxazine
Surface free energy

ABSTRACT

We have prepared semi-interpenetrating polyacrylate networks (PA/BA-m s-IPNs) through rapid photopolymerization of a triacrylate monomer (TMPTA) in the presence of a photoinitiator (I184), a tetramercaptane transfer agent (4SH), and *N*-methyl-bisbenzoxazine (BA-m). Next, we prepared novel fully interpenetrating polyacrylate (PA) and polybenzoxazine (PBZ) networks (PA/PBZ f-IPNs) through thermal polymerization of the BA-m monomer at 180 °C for 4 h. For the PA/BA-m s-IPNs, the BA-m monomers can be frozen and dispersed in the UV-cured PA network within 5 min to inhibit macrophase separation. After thermal polymerization, the phenol units of the ring-opened PBZ segments can form a hydrogen-bonding interface with the carbonyl groups to improve the compatibility between the PBZ microdomains and the PA networks. From an analysis using Kissinger's method, the non-isothermal kinetics of the thermal polymerization for the PA/BA-m s-IPNs indicate that an increase in the PA content increased the steric hindrance of PBZ polymerization. We used DSC, TGA, and contact angle analyses to determine the glass transition temperature, thermal stability, and surface free energy, respectively, of the PA/PBZ f-IPNs. The thermal stability and surface free energy of these PA/PBZ f-IPNs display linear relationships with respect to the PBZ content.

1. Introduction

In polymer blends, high-molecular-weight polymers have extremely low mixing entropy, usually resulting in macrophase separation [1,2]. Thus, the interfacial compatibility of a polymer blend incorporating two or more components plays an important role in determining its performance. Thermodynamically, the presence of hydrogen-bonding interactions between proton-donor and -acceptor polymers can improve the miscibility of their blend, resulting in either microphase separation or total miscibility [3,4]. The use of interpenetrating polymer networks (IPNs) is another method of achieving microphase-separated polymer blends through the polymerizing or crosslinking at least one component of the composite polymer in the presence of the other [5,6]. The size of phase separation domains when using the IPN method depends on the polymerization rate and the strength of the intermolecular interactions between the components. Thus, rapid polymerizations, such as UV-curing, are necessary to form relatively small microphase separation domains within IPNs [7,8]. Under intense UV illumination, photolysis of photoinitiators can generate reactive free radicals that are capable of mediating the crosslinking polymerization of liquid multi-vinyl monomers into high-molecular-weight polymeric solids. For thiol-ene photopolymerizations, thiol additives can behave as reversible radical transfer agents to reduce oxygen-induced inhibition for UV-curing reactions performed in air [9–11].

The hydrophobic and oleophobic surfaces of low-surface-free energy coating materials are useful for applications in, for example, aerospace, lithography, sports, outdoor clothing, biomedical layers, integrated sensors, and protection against environmental fouling [12–16]. In a reversible isothermal process, the surface free energy is equal to the work required to form a new unit surface when separating two phases that remain in equilibrium [17]. Generally, the surface free energy (γ) of a homogenous solid surface can be divided into a constitutive effect and a density (morphological) effect [18,19]. The constitutive law states that surfaces having similar surface chemical compositions will have similar surface tensions. The surface free energy (units: mJ/m^2) of constituent groups decreases in the order CH_2 (36) > CH_3 (30) > CF_2 (23) > CF_3 (15) [20–23]. Because the densities of crystalline and crosslinking polymers are usually higher than that of amorphous polymers, their surface free energies are usually much higher than those of

* Corresponding author. Tel./fax: +886 3 5131512.
E-mail address: changfc@mail.nctu.edu.tw (F.-C. Chang).

0032-3861/$ – see front matter Crown Copyright © 2008 Published by Elsevier Ltd. All rights reserved.
doi:10.1016/j.polymer.2008.09.004

amorphous polymers (cf. 35.7 mJ/m^2 for amorphous PE and 66.8 mJ/m^2 for 96.3% crystalline PE) [18]. The well-known polytetrafluoroethylene (Teflon™) is considered to be the "benchmark" low-surface-free energy material because it combines water repellence [18] with other desirable properties [24]. Unfortunately, the use of Teflon comes with certain disadvantages, such as those resulting from its low oil repellence, high cost, and poor processability. Considerable research efforts have, therefore, been directed toward the development of other low-surface-free-energy polymeric materials that exhibit good film-forming characteristics [25,26].

Polybenzoxazine (PBZ) resins [27,28] possess several unusual properties (and applications), such as near-zero shrinkage during polymerization (thin-film formation) [29,30], high char yields (fire retardation) [31–34], low-surface-free energies (self-cleaning coatings) [35–38], and high glass transition temperatures (heat-resistant resins). Benzoxazine monomers are usually prepared at 100 °C through the Mannich reaction (dehydration and addition) between a phenol ($R_2C_6H_4OH$), an amine (R_1NH_2), and formaldehyde or paraformaldehyde (Scheme 1a) [27]. The choice of the phenol and amine partners permits the design of monomers exhibiting flexibility and the tailoring of the PBZ polymer properties. Upon heating to 150 °C, the C–O bonds of the benzoxazine rings cleave heterogeneously into carbocations [39] and phenoxide anions [39,40], which transform into a polymer constituting ortho-substituted phenol units (aminoalkylation of phenoxide anions) [41,42], as indicated in Scheme 1b. The catalyst- and byproduct-free bulk polymerizations of PBZ are the major advantages of using this approach relative to those performed with other thermosetting polymers [27]. A high curing temperature (>120 °C) is necessary, however, to cleave the C–O bonds on the benzoxazine ring when forming aromatic ortho-substituted PBZ polymers [27,37]. From in-depth characterizations of model benzoxazine oligomers using ^{1}H, ^{13}C NMR, and FTIR spectroscopy, Kim and Ishida revealed that a pseudo-cyclic structure based on stable intramolecular [–O$^-$⋯HN$^+$–] ionic interactions (see Scheme 1c) results in the possibility of helical structure formation in longer-chain benzoxazine oligomers [43]. This observation has also been supported by solid state NMR [44,45] and powder XRD [46] analyses. The hydrophobic surfaces of PBZ resins (water contact angle: 114°; cf. 116° for smooth Teflon [47] and 104° for smooth i-PP [48]) can be also attributed to this unique intermolecular interaction, which induces the hydrophobic methyl groups (cf. $\gamma = 30.1$ mJ/m^2 for amorphous PP [18]) to be positioned on the outside of the helical microstructures [30]. Industrial applications of PBZ resins are restricted, however, by their glass-like brittle mechanical properties. Therefore, decreasing the brittleness of PBZ resins would be a major advance toward obtaining low-surface-free energy coatings on flexible substrates [27].

Two-component hydrogen-bonding polymer blends of PBZ and carbonyl proton-acceptor polymers, such as poly(ε-caprolactone) [49] and polycarbonate [50], form two microdomains that are connected through a hydrogen-bonding interface that uses the phenol units as proton-donors. This phase separation is due to the intramolecular interactions between the PBZ segments being stronger than those between the PBZ segments and the blended polymer chains, as evidenced by the shift in the wavenumber of the signal for the non-bonding hydroxyl groups in FTIR spectra (i.e., free –OH at 3525 cm^{-1}, –O$^-$⋯HN$^+$– at 2795 cm^{-1} for pure PBZ [35], and –OH⋯O═C at 3385 cm^{-1} for PBZ/PCL blends [49]). In this present study, we prepared a series of well-dispersed fully interpenetrating polymer networks (PA/PBZ f-IPNs) through two-step polymerization: (i) photopolymerization of a trifunctional acrylate (TMPTA) in the presence of a photoinitiator (I184) and a reversible radical transfer agent (4SH) at 25 °C for 10 min and (ii) thermal polymerization of a bisbenzoxazine monomer (BA-m) at 180 °C for 4 h. For semi-interpenetrating polymer networks (PA/BA-m s-IPNs), we used a DSC-assisted kinetic study to investigate the steric hindrance effect during the thermal polymerization in the PA network. The hydrogen-bonding interface between the PA networks and the PBZ domains was investigated using temperature-dependent FTIR spectroscopy. Photographic and FESEM images revealed that the components of the PA/BA-m s-IPN or PA/PBZ f-IPNs were mixed well. The thermal properties of the PA/PBZ f-IPNs, including their glass transition temperatures (T_g), thermal degradation temperatures (T_d), and char yields, were analyzed from

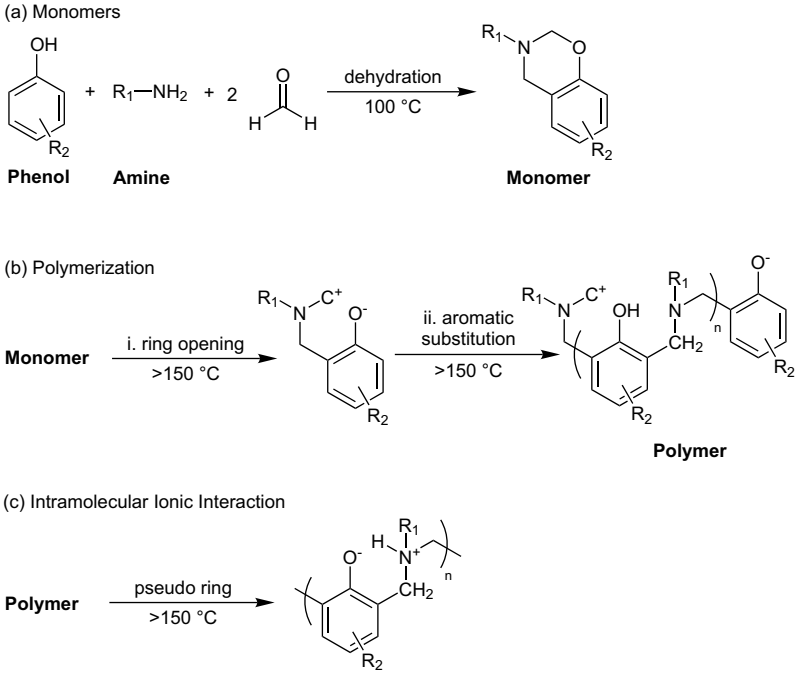

Scheme 1. Synthesis of benzoxazine monomers and polymers; intramolecular ionic interaction between phenol and tertiary amine units.

TGA and DSC thermograms. The surface free energies of the PA/PBZ f-IPNs were obtained from contact angle analyses and the three-liquid acid/base method.

2. Experimental section

2.1. Materials

The triacrylate monomer trimethylolpropane triacrylate (TMPTA) and the reversible radical transfer agent pentaerythritol tetrakis(3-mercaptopropionate) (4SH) were purchased from Sigma–Aldrich. The photoinitiator Irgacure 184 (I184) was purchased from Ciba Specialty Chemicals. The bisbenzoxazine monomer 2,2-bis(3,4-dihydro-3-methyl-2*H*-1,3-benzoxazine)propane (BA-m) was supplied by Shikoku Corp. Deionized water, ethylene glycol (≥99%; Aldrich), and diiodomethane (99%; Aldrich) were used as standards to measure the surface free energies. All chemicals were used as-received.

2.2. Measurements

A Nicolet Avatar 320 FTIR spectrometer (32 scans; resolution of 1 cm^{-1}; nitrogen purge; temperature-controlled using a hot stage) was used to record FTIR spectra of the samples from KBr disks. The films of the PA/PBZ f-IPNs (Fig. 6) were fractured in liquid nitrogen and the interface morphology was examined using a Hitachi S-4800 FESEM (Fig. 7). A DuPont DSC-9000 calorimeter (scan rate: 20 °C/min; scan range: from −100 to 180 °C) was used to record DSC thermograms of samples (ca. 5–10 mg) sealed in aluminum pans. The temperature and energy were indium calibrated. The glass transition temperature was obtained from the midpoint of the specific heat increment. A TA Instruments thermogravimetric analyzer (scan rate: 20 °C; scan range: 30–800 °C; nitrogen purge: 40 mL/min) was used to record TGA thermograms of samples placed on a Pt holder. The advancing contact angles of liquids (5 μL) on the polymer samples were measured at 25 °C using a Krüss GH-100 goniometer interfaced with image-capture software. To obtain reliable contact data, at least three droplets were dispensed at different regions of the same piece of film, and at least two pieces of film were used to obtain reliable contact angle data. Thus, at least six advancing contact angles were averaged for each kind of film and each kind of liquid. Deionized water, ethylene glycol (≥99%; Aldrich), and diiodomethane (99%; Aldrich) were used as standards to measure the surface free energies.

2.3. Surface free energy determination

In the modern theory of surface science, Fowkes [51,52] proposed that the surface free energy (γ) can be resolved into several components due to the (London) dispersion force (γ^{d}), the (Keesom) dipole–dipole interaction (γ^{dip}), the (Debye) induction force (γ^{din}), and hydrogen bonding (γ^{h}):

$$\gamma = \gamma^{d} + \gamma^{dip} + \gamma^{ind} + \gamma^{h} \quad (1)$$

By rearranging this equation to

$$\gamma = \gamma^{LW} + \gamma^{AB} \quad (2)$$

van Oss and Good expressed the surface energy as

$$\gamma^{LW} = \gamma^{d} + \gamma^{dip} + \gamma^{ind} \quad (3)$$

where LW stands for Lifshitz–van der Waals. Because a hydrogen bond is a proton-sharing interaction between an electronegative molecule or group and an electropositive hydrogen atom, van Oss and Good [53,54] considered it to be as an example of an interaction between a Lewis acid (electron acceptor) and a Lewis base (electron donor). In addition, they created two new parameters, as shown in Eq. (4), to redefine the γ^{AB} interaction to quantify its strength: γ^{+} and γ^{-}, the Lewis acid and base parameters of the surface free energy.

$$\gamma^{AB} = 2\sqrt{\gamma^{+}\gamma^{-}} \quad (4)$$

$$\gamma = \gamma^{LW} + 2\sqrt{\gamma^{+}\gamma^{-}} \quad (5)$$

Using Eq. (5), van Oss, Good, and co-workers developed a "three-liquid procedure" [55] to determine the solid surface free energy (γ_S) from contact angle measurements and the traditional Eq. (6):

$$\gamma_L(1+\cos\theta) = 2\left(\sqrt{\gamma_S^{LW}\gamma_L^{LW}} + \sqrt{\gamma_S^{+}\gamma_L^{-}} + \sqrt{\gamma_S^{-}\gamma_L^{+}}\right) \quad (6)$$

To determine the value of γ_S of a polymer solid, diiodomethane, ethylene glycol, and water are usually selected as representative apolar and polar liquids. When the parameters γ_L, γ^{LW}, γ^{+}, and γ^{-} of the three liquids in Eq. (6) are available, the parameters γ_S^{LW}, γ_S^{+}, and γ_S^{-} of the surface can be determined through contact angle measurements by solving three simultaneous equations. The solid surface free energy (γ_S) can be determined from Eq. (5).

2.4. Blends and procedures

The two components for UV-curing and thermal polymerization were prepared separately as solutions in THF (20 wt%) and then they were blended at various weight ratios. For UV-curing, the triacrylate monomer (TMPTA, 10 g), the reversible radical transfer agent (4SH, 0.2 g), the photoinitiator (I184, 0.4 g), and the solvent (THF, 50 g) were added in a 100-mL sample bottle. For thermal polymerization, a mixture of the bisbenzoxazine monomer (BA-m, 10 g) and THF (50 g) was purified by filtration through a 0.2-μm syringe filter into a 100-mL sample bottle. Three-step procedures were used to prepare PA/PBZ f-IPNs: (i) drying in a convection oven at 60 °C for 20 min, (ii) photopolymerization under 254-nm UV light [CL-1000 crosslinker (UVP Inc.)] at 25 °C for 5 min, and (iii) thermal polymerization in a convention oven at 180 °C for 4 h.

3. Results and discussion

3.1. Two dissimilar polymerizations of PA/PBZ f-IPNs

Semi-interpenetrating polymeric networks (PA/BA-m s-IPNs) were prepared through photopolymerization (Scheme 2a) of a triacrylate monomer (TMPTA) in the presence of a photoinitiator (I184) and a reversible transfer agent (4SH) and a bisbenzoxazine monomer (BA-m). The I184 photoinitiator was decomposed into initiating free radicals under 254-nm UV light and then the tetramercaptane agent (4SH) was reversibly transferred the free radicals to prevent surface oxygen inhibition [9–11]. These UV-induced free radicals initiated the polymerization of TMPTA into the polyacrylate (PA) network. During the thermal ring-opening polymerization of the PA/BA-m s-IPNs, the C–O bonds of the *N*-methyl-bisbenzoxazine monomer (BA-m) in the PA network cleaved into carbocations [39] and phenoxide anions [39,40], which reacted with the ortho-positions of the benzoxazine units (aminoalkylation of phenoxide anions [41,42]) to form fully interpenetrating polyacrylate and polybenzoxazine networks (PA/PBZ f-IPNs) constituted by ortho-substituted phenol linkages (Scheme 2b). Table 1 lists the compositions and thermal properties of the PA/PBZ f-IPNs, including their glass transition temperatures (T_g), thermal decomposition temperatures (T_d at 5 wt%), and char yield at 700 °C. We

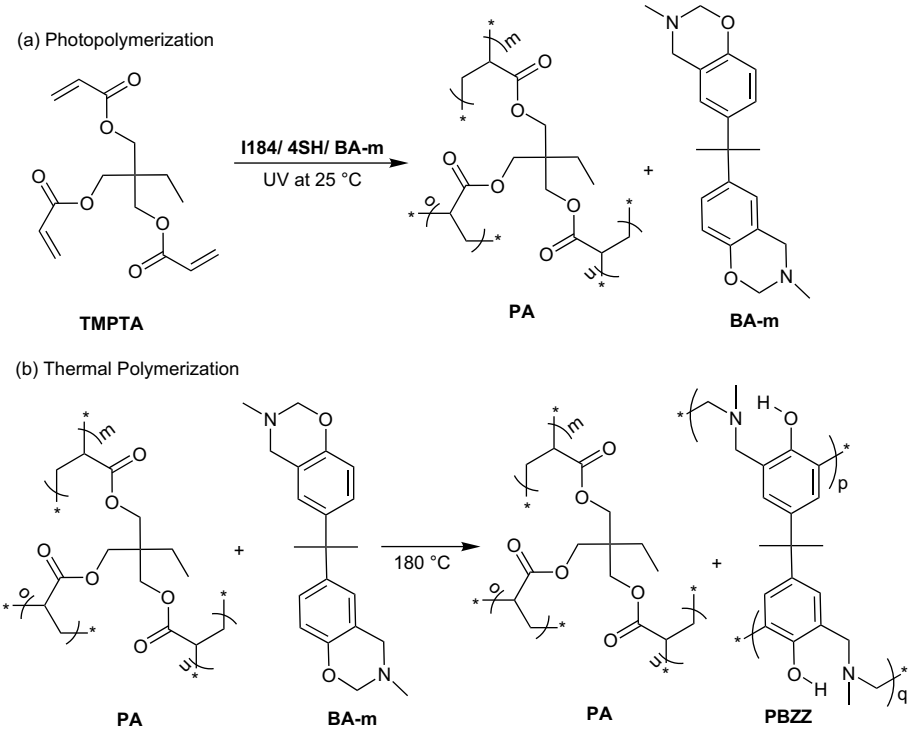

Scheme 2. Preparation of PA/PBZ f-IPNs: (a) Photopolymerization of triacrylate monomer (TMPTA) with a photoinitiator (I184) and a reversible radical transfer agent (4SH); (b) thermal ring-opening polymerization of *N*-methyl-bisbenzoxazine monomer (BA-m).

combined photopolymerization and thermal polymerization for the preparation of the PA/PBZ f-IPNs because of three factors: (i) The UV absorbance of BA-m at 254 nm is extremely low relative to that of the photoinitiator I184; therefore, most of the photons induced decomposition of I184 to form initiating radicals for the photopolymerization of TMPTA. In contrast, the photopolymerization of TMPTA with the *N*-phenyl-bisbenzoxazine monomer BA-a did not occur because of the strong UV absorbance of aniline derivatives at 254 nm. (ii) Generally phenol groups are regarded as free radical inhibitors; the addition of 1 wt% of a phenol monomer can effectively suppress photopolymerization. In the benzoxazine monomer, the six-membered rings function as protective groups for photopolymerization. (iii) The low degree of shrinkage during the thermal polymerization can maintain the shape of the UV-cured PA/BA-m s-IPNs [29,30].

3.2. Steric effect of PBZ polymerization in PA network

Upon heating to 250 °C at a rate of 20 °C/min, the DSC thermogram (Fig. 1a) reveals that the onset of exothermic polymerization of the 100% BA-m PA/BA-m s-IPNs began at 160 °C with a maximum exothermic peak (T_p) at 220.8 °C. In contrast, the values of T_p for the PA/BA-m s-IPNs containing 60, 50, and 40% BA-m were 227.7, 230.6, and 234.5 °C, respectively (Fig. 1b–d). In addition, tailing of the exothermal peaks to temperatures below 160 °C resulted from the autopolymerization of residual acrylate monomers at the onset temperature of 120 °C (Fig. 1e). Curing reactions of PBZ at temperatures below and above T_g revealed kinetics that were significantly different. Vitrification (glassy state) occurred sooner at higher cure temperatures than at lower ones, especially those below the value of T_g [27]. We attribute this temperature effect to the fact that temperatures higher than T_g can suppress both inter- and intramolecular hydrogen bonding, which are greatly susceptible to steric hindrance for ortho substitution (alkylamination). To achieve successful processing, the cure kinetics of PA/BA-m s-IPNs were investigated using DSC, which indicated that the curing of the benzoxazine components was an autocatalyzed

Table 1
Compositions and thermal properties of PA/PBZ f-IPNs

Entry	BA-m/TMPTA/I184/4SH (wt%)	T_g[a] (°C)	T_d[b] (5%) (°C)	Char Yield[c] (wt%)
0% BA-m	0/94.34/1.89/3.77	N.A.	422.3	4.9
20% BA-m	20/75.47/1.51/3.02	N.A.	367.4	14.1
40% BA-m	40/56.60/1.13/2.26	196.5	316.8	20.5
50% BA-m	50/47.17/0.94/1.89	193.7	304.7	23.4
60% BA-m	60/38.46/0.51/1.03	192.2	294.8	27.1
80% BA-m	80/18.87/0.38/0.75	191.3	288.8	31.7
100% BA-m	100/0/0/0	181.3	288.9	36.7

[a] Determined from two baselines before and after glass transition.
[b] Measured at 5 wt% loss.
[c] Measured at 700 °C.

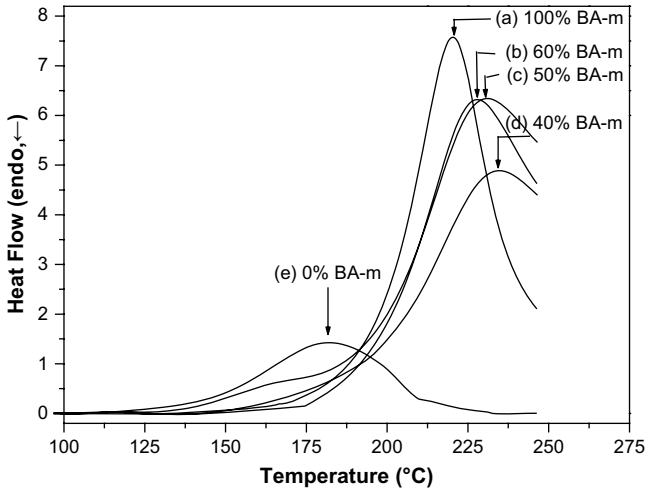

Fig. 1. DSC thermograms of PA/BA-m s-IPNs incorporating (a) 100, (b) 60, (c) 50, (d) 40, and (e) 0% BA-m; heating rate: 20 °C/min.

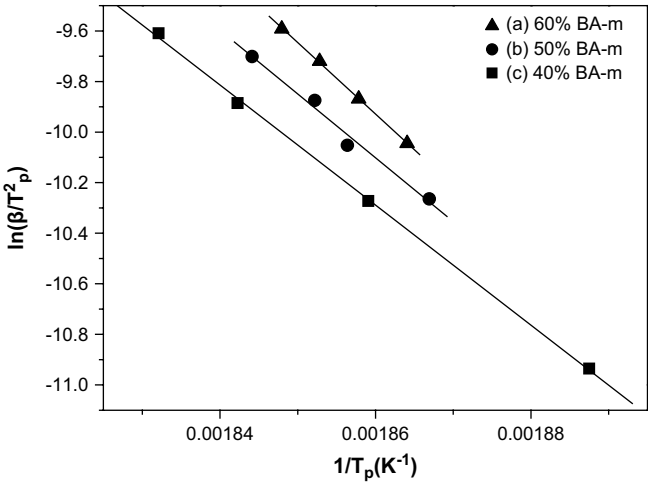

Fig. 2. Kissinger plots of the exothermic polymerization peaks (T_p) obtained at DSC heating rates (β) of 5–20 °C/min for PA/BA-m s-IPNs incorporating (a) 60, (b) 50, and (c) 40% BA-m.

reaction until vitrification (glassy state) occurred, when diffusion began to control the curing process [56,57]. In general, the specific heat must be a constant or vary linearly with respect to the scanning temperature to generate kinetic data for more convenient non-isothermal experiments using DSC methods. Fig. 2 and Table 2 reveal that the non-isothermal experimental data of PA/BA-m s-IPNs are in good agreement with Kissinger's hypothesis (i.e., $R^2 =$ ca. 0.9993 for 40% BA-m PA/BA-m s-IPNs). Under a constant heating rate β (i.e., dT/dt), the heat flow dH/dt (which equals H_{100}[d$(1-\alpha)$/dt]) in the DSC thermogram is proportional to the polymerization rate dM/dt (which equals M_0[d$(1-\alpha)$/dt]), where T is the reaction temperature, t is the reaction time, H is the reaction enthalpy at a given monomer conversion of α, M is the monomer concentration at a given monomer conversion of α, and the suffixes 100 and 0 refer to conditions of 100 and 0% monomer conversions ($\alpha = 1$; $\alpha = 0$), respectively. Based on the Kissinger method, the activation energy (E_a) and Arrhenius pre-exponential factor (A) can be obtained when the polymerization acceleration rate is zero at the exothermic peak temperature (T_p) under a given heating rate (β). The resulting relation can be expressed by Eq. (7), where R is the universal gas constant. The values of E_a and A correspond to (i) the activation energy of the ring opening of the benzoxazine rings (C–O) to give phenoxide anions and carbocations and (ii) the steric effect of ortho substitution of the phenoxide units with nearby carbocations during the thermal polymerization of the BA-m monomers. The similar slopes (E_a/R) of the Kissinger plots [$\ln(\beta/T_p^2)$ vs. $1/T_p$] indicate that the activation energy (E_a) of the ring opening of the benzoxazine rings is independent on the PA content. Relative to the value for the polymerization of the 40% BA-m PA/BA-m s-IPN, the Arrhenius pre-exponential factors (A) for the PBZ polymerizations of the 50 and 60% BA-m PA/BA-m s-IPNs were 20- and 7000-fold higher, respectively. This finding provides evidence that the steric hindrance of the PA medium resulted in the shift of the maximum exothermic peak (T_p) in Fig. 1.

$$\ln\left(\frac{\beta}{T_p^2}\right) = \ln\left(\frac{AR}{E_a}\right) - \frac{E_a}{RT_p} \tag{7}$$

3.3. Intra- and intermolecular interaction

The IR spectrum of the 100% BA-m PA/PBZ f-IPN (pure PBZ resin in Fig. 3) reveals signals for the intramolecular [O⁻···HN⁺] ionic interaction at 2795 cm^{-1}, the intramolecular [OH···N] hydrogen bond at 3120 cm^{-1}, and the intermolecular [OH···N] or [OH···O] hydrogen bond at 3382 cm^{-1}, where the intramolecular interactions are physical bonds possessing pseudo-six-membered rings (see the inserted chemical structure in Fig. 3). Coleman et al. used the wavenumber difference ($\Delta\nu$) between the bonded and free hydroxyl stretching modes to investigate the average strength of the intermolecular interactions [1,2]. The relatively large shifts in the signals of the intramolecular [O⁻···HN⁺] and [OH···N] interactions ($\Delta\nu = 745$ and 420 cm^{-1}, respectively) in the pseudo-six-membered rings relative to the position of the free O–H modes at 3540 cm^{-1} are consistent with their high strength compared with the weak [O⁻···HN⁺] and [OH···N] intermolecular hydrogen bonds ($\Delta\nu = 158$ cm^{-1}). Thus, most of the segments of PBZ exist in the form of intramolecular [O⁻···HN⁺] interactions, which is consistent with its low miscibility with other proton-acceptor polymers, such as PCL, PC, and PEO [49,50,53–55]. Nevertheless, intermolecular hydrogen bonding between PA and PBZ could still be observed in FTIR spectra (Fig. 4). Upon decreasing the BA-m content, the free and [OH···O=C] modes appear at 3524 and 3407 cm^{-1} for PA/PBZ f-IPNs because of the greater interface between the PBZ domains and the PA networks. Fig. 5 and Table 3 present the carbonyl stretching mode and two fitted Gaussian curves ranging from 1680 to 1780 cm^{-1} for PA/PBZ f-IPNs of various compositions. The carbonyl stretching wavenumber split into two bands at 1736 and 1721 cm^{-1}, corresponding to the signals of free and hydrogen-bonded carbonyl groups (cf. $\Delta\nu = 20$ cm^{-1} for PCL/PBZ [49]). The fraction of hydrogen-bonded carbonyl groups can be calculated using Eq. (8), where the absorptivity ratio of the FTIR spectroscopic absorption at 1736 and 1721 cm^{-1} is 1.5, according to previous studies of hydroxyl–carbonyl intermolecular association [60]. The terms A_F and A_{HB} denote the Gaussian peak areas corresponding to the free and hydrogen-bonded carbonyl groups, respectively. The fractions of hydrogen-bonded carbonyl groups for

Table 2
Kissinger parameters of PBZ polymerization for PA/PBZ s-IPNs

Entry	ln(AR/E_a)	E_a/R	R^2	E_a[a]	A[b]
40% BA-m	33.87	-2.37×10^4	0.9993	-1.97×10^5	-1.22×10^{19}
50% BA-m	36.83	-2.52×10^4	0.9839	-2.10×10^5	-2.51×10^{20}
60% BA-m	42.58	-2.82×10^4	0.9996	-2.35×10^5	-8.81×10^{22}

[a] Units of J/mol.
[b] Units of K.

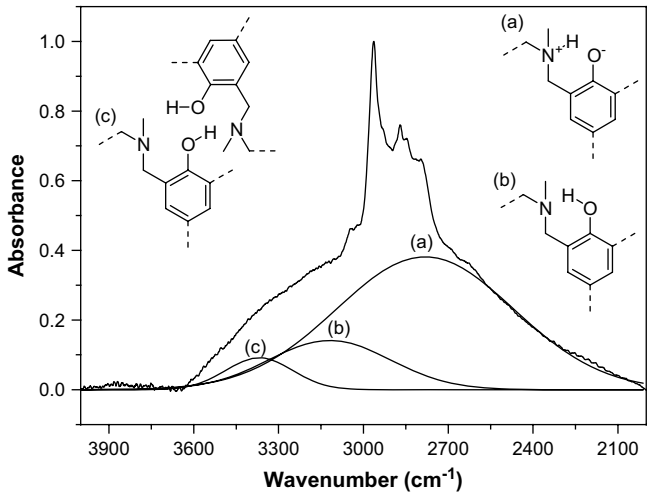

Fig. 3. Hydroxyl stretching region in the FTIR spectrum of 100% BA-m PBZ and its Gaussian fitting curves for the (a) intramolecular ionic [O⁻···HN⁺] interaction at 2795 cm^{-1}, (b) the intramolecular [OH···N] hydrogen bond at 3120 cm^{-1}, and (c) the intermolecular [OH···N] or [OH···O] hydrogen bond at 3382 cm^{-1}.

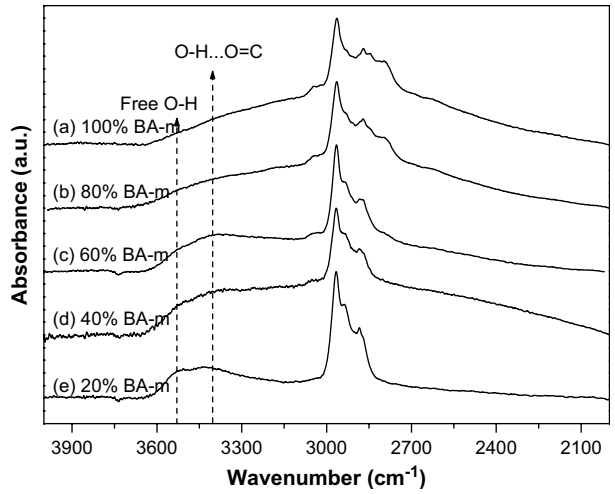

Fig. 4. Hydroxyl stretching region (4000–2000 cm^{-1}) of the FTIR spectra of PA/PBZ f-IPNs incorporating (a) 100, (b) 80, (c) 60, (d) 40, and (e) 20% BA-m.

the 40, 60, and 80% BA-m PA/PBZ f-IPNs were 7.89, 14.41, and 18.68%, respectively. In comparison with the corresponding values reported in the literature [49,57–60] for PCL/PBZ, PCL/novolac, PCL/epoxy, and PCL/phenoxy blends, the low fraction of hydrogen-bonded carbonyl groups in the PA/PBZ f-IPNs is due to the presence of intramolecular ionic [$O^{-}\cdots HN^{+}$] interactions and a network

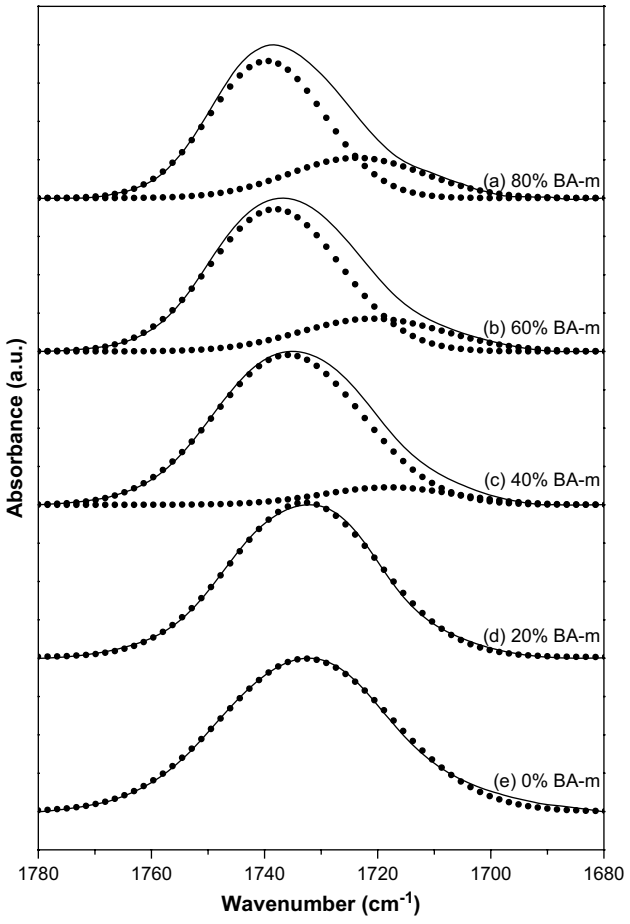

Fig. 5. Carbonyl stretching region (1780–1680 cm^{-1}) in the FTIR spectra of PA/PBZ f-IPNs incorporating (a) 80, (b) 60, (c) 40, (d) 20, and (e) 0% BA-m.

Table 3
Curve-fitting data of carbonyl groups for PA/PBZ f-IPNs

Entry	Free C=O		H-Bonded C=O		f (%)
	ν_F (cm^{-1})	A_F	ν_{HB} (cm^{-1})	A_{HB}	
0% BA-m	1733	37.87	–	–	–
20% BA-m	1733	33.18	N.A.	N.A.	N.A.
40% BA-m	1736	25.92	1718	3.33	7.89
60% BA-m	1738	26.81	1721	6.77	14.41
80% BA-m	1740	22.72	1724	7.83	18.68

A_F: integral area of free C=O; A_{HB}: integral area of bonding C=O; ν_F: wavenumber of free C=O; ν_{HB}: wavenumber of bonding C=O; f: fraction of bonded C=O determined using the expression $(A_{HB}/1.5)/(A_F + A_{HB}/1.5) \times 100\%$ (correct to 1.5).

effect. Herein, the irreversible PBZ crosslinking and the immobile PA network reduce the miscibility of PBZ in the PA matrix and force the PBZ component to phase separate from the restricted network.

$$f(\%) = \frac{A_{HB}/1.5}{A_{HB}/1.5 + A_F} \times 100\% \quad (8)$$

3.4. Appearance and microstructures

Fig. 6 presents images of the transparent films of the PA/BA-m s-IPNs (a–c) and PA/PBZ f-IPNs (d–f) incorporating 40, 50, and 60% BA-m. These transparent films suggest that the blends of two components were mixed well in the s- and f-IPNs. Therefore, we can observe phase separation on the fracture surface using SEM images because only relatively weak [OH···O=C] bonds exist between the PA and PBZ rigid domains [61]. Under kinetic control, the rapid photopolymerization of TMPTA can freeze BA-m in the PA network to inhibit the macrophase separation during the following thermal polymerization. Thus, the FESEM cross-sectional images (Fig. 7) of the PA/PBZ f-IPNs reveal that the diameters of the dispersed hard PBZ domains (white dots) were, on average, smaller than 100 nm (cf. the large aggregates in the PU/PBZ blends [61]). In comparison with the 60% BA-m PA/PBZ f-IPN, the size and distribution of the PBZ domains were smaller and more dispersed for the 50 and 40% BA-m PA/PBZ f-IPNs. Under the same sample preparation conditions, less crazing of the 40% BA-m PA/PBZ f-IPN occurred on the fracture interface, indicating that the incorporation of PA networks through rapid photopolymerization improved the miscibility of the two components.

3.5. Thermal properties

Ishida and Allen performed a comparative investigation of several of the physical properties of PBZs prepared through thermal curing of BA-a and BA-m difunctional monomers [29]. Despite low crosslinking densities (52% conversion of benzoxazine rings for the polymerization of BA-a at 180 °C for 4 h [57]), the PBZ materials exhibited high glass transition temperatures (T_g = 150 °C for BA-a and 180 °C for BA-m) because of their unique intramolecular [$O^{-}\cdots HN^{+}$] interactions [43–46]. As mentioned above our discussion of the steric effect, vitrification (glassy state) occurred more rapidly at curing temperatures higher than the glass transition temperatures. In other words, PBZ polymerization is suppressed by thermal motion of PBZ (T_g = ca. 180 °C), resulting in glass transition temperatures similar to those in the PA/PBZ f-IPNs (e.g., 182 °C for 100% BA-m and 192 °C for the other compositions in Fig. 8). The increase in the value of T_g by 10 °C can be attributed to the steric hindrance of the PA network. For methylamine-type PBZ (BA-m monomers), the methyl groups on the nitrogen atoms are readily oxidized, decomposing (deaminomethylation) at temperatures (T_d)

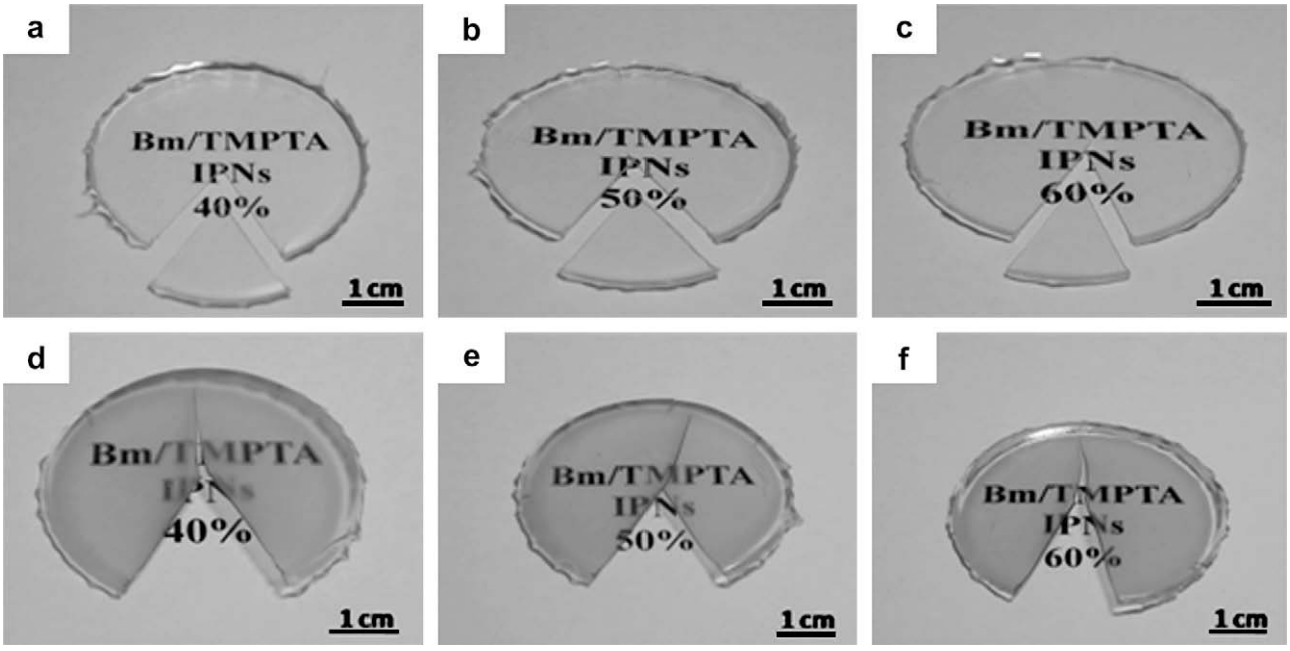

Fig. 6. Photographs of (a–c) PA/BA-m s-IPNs and (d–f) PA/PBZ f-IPNs incorporating (a, d) 40, (b, e) 50, and (c, f) 60% BA-m.

above 250 °C [cf. T_d above 300 °C for aniline-type PBZ (BA-a monomers)] [62]. During the second event at ca. 400 °C, the isopropylidene linkages of the bisphenol A units were cleaved. We attributed the final weight loss, centered near 460 °C, to the formation of a char, with the release of traces of phenolic and a significant amount of substituted benzene compounds [62]. Fig. 9a and Table 1 provide the thermal properties of the PA/PBZ f-IPNs. Both the decomposition temperatures at 5 wt% loss and the char yields at 700 °C are close to the weight-average values between 0% BA-m and 100% BA-m for all compositions of the well-mixed PA/PBZ f-IPNs (Fig. 9b). In comparison with 100% BA-m (T_d = ca. 288.9), the thermal stability of the 40% BA-m PA/PBZ f-IPN was increased by 27.9–316.8 °C.

3.6. Surface properties

The intramolecular ionic [$O^-\cdots HN^+$] interaction results in helical microstructures, which induce the hydrophobic methyl groups to be located on the surface [43–46]. Thus, the surface characteristics of PBZ should be close to those of polypropylene (PP). According to theoretical and experimental studies [18], amorphous and high-molecular-weight PBZs possess lower surface free energies than do crystal PPs ($\gamma_S = 39.5$ mJ/m^2 for i-PP and 28.0 mJ/m^2 for a-PP). In addition, the helical conformation influenced by strong intramolecular [$O^-\cdots HN^+$] interactions is also an important factor for the polymer's near-zero shrinkage because of simultaneous increases in the number of chemical bonds

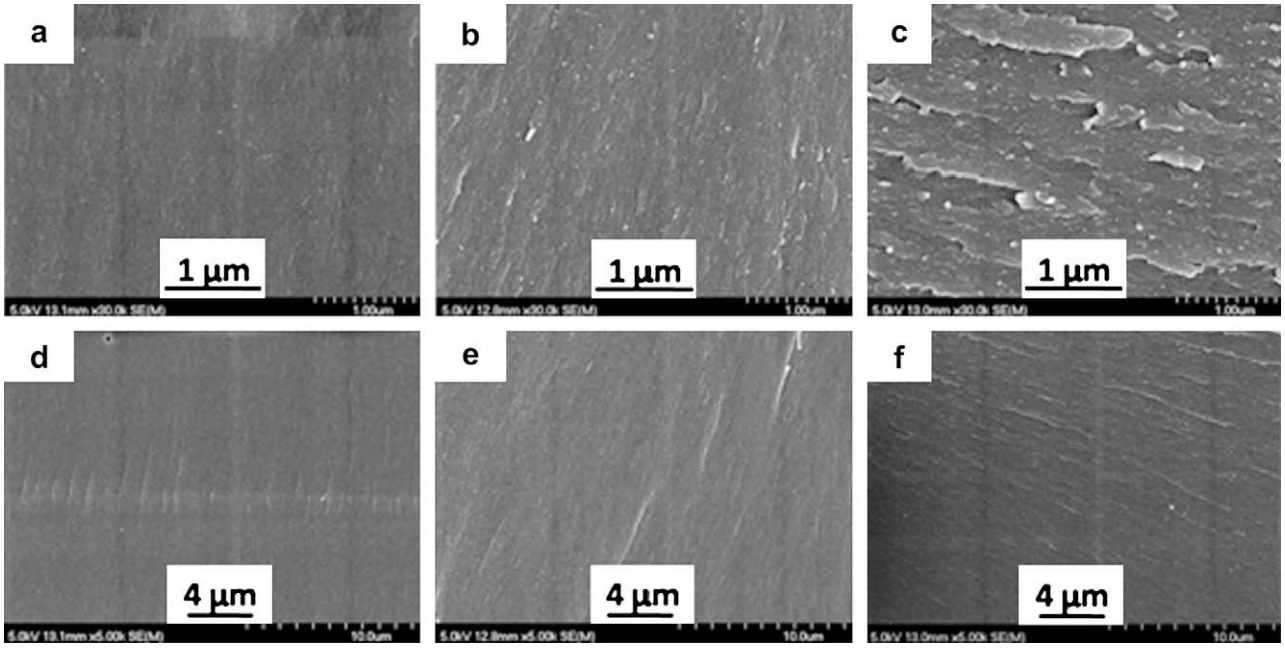

Fig. 7. FESEM cross-sectional images of PA/PBZ f-IPNs incorporating (a, d) 40, (b, e) 50, and (c, d) 60% BA-m.

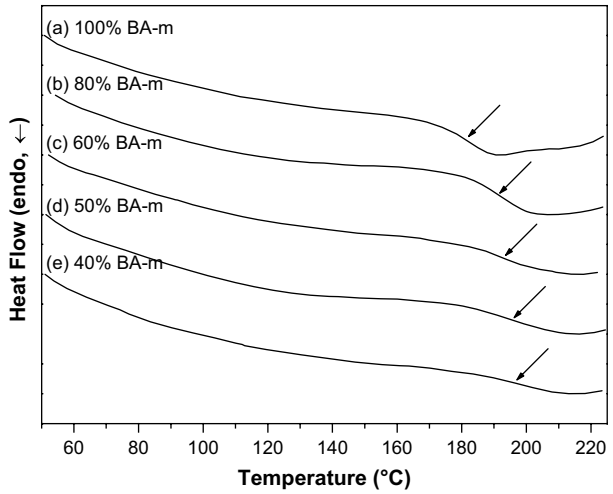

Fig. 8. DSC thermograms of PA/PBZ f-IPNs incorporating (a) 100, (b) 80, (c) 60, (d) 50, and (e) 40% BA-m.

(networks) and intermolecular distances (free volumes, polymer density) [29,30]. Table 4 lists the surface elemental compositions of the 100% BA-m monomer solution spin coated onto wafers after plasma [63] and heat [35] treatments. In comparison with the theoretical nitrogen content of 8 mol%, we did not observe any surface nitrogen components in the ESCA spectra of the BA-m monomers or the ring-opened PBZ polymers, presumably because of the screening of the benzoxazine rings or the $[O^{-}\cdots HN^{+}]$-induced pseudo-six-membered rings of the polymers. After high-energy Ar plasma treatment for 15 min, the surface BA-m monomers were ring opened, resulting in the ESCA spectra revealing a nitrogen content of 3.98 mol% [63]. After subsequent heat treatment at 210 °C for 1 h, the surface nitrogen content remained at 4.43 mol%. These observations support the hydrophobic character of the PBZ surface. Table 5 lists the surface free energy parameters of the PA/PBZ f-IPNs. The surface free energy of a solid film is usually obtained from the contact angles of selective liquids, such as water, diiodomethane, and ethylene glycol; hydrophobic and oleophobic surfaces are characterized by a water contact angle greater than 100° and a diiodomethane contact angle greater than 60°, respectively. We used van Oss and Good's three-liquid LWAB method to calculate a surface free energy (γ_S) of 24.8 mJ/m^2 for the 100% BA-m PA/PBZ IPN. This value approaches that typically observed for Teflon ($\gamma_S = 21$ mJ/m^2) under the same conditions. We obtained a lower surface free energy (γ_S) of 16.5 mJ/m^2 after thermal polymerization of this material at 210 °C for 1 h, i.e., after more ring-opened PBZ segments were created in the form of $[O^{-}\cdots HN^{+}]$ units [35]. The surface free energies (γ_S) of the PA/PBZ f-IPNs prepared at other compositions depended on the BA-m content (Fig. 10). In general, low-energy additives can migrate to a solid surface to drastically lower its surface tension [18]. We found, however, that the PBZ microdomains were well dispersed in the PA medium as a result of [OH···O=C] hydrogen bonds. This result is reasonable for PA/PBZ f-IPNs having surface free energies that are similar to those of its bulk thermal properties. In comparison with the 100% BA-m, the surface free energy of the 40% BA-m PA/PBZ f-IPN was increased slightly by 2.6–27.4 mJ/m^2.

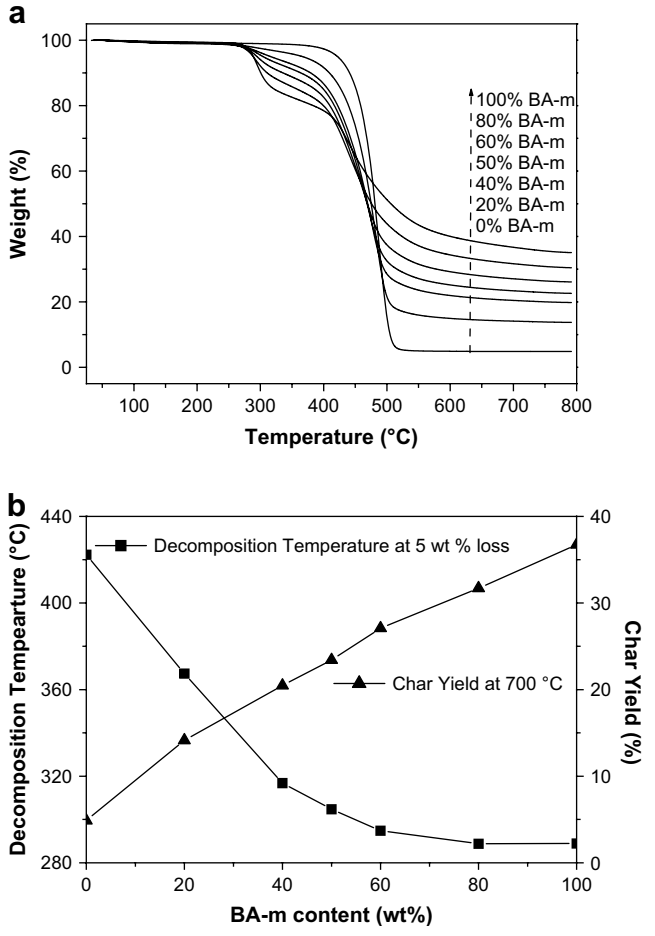

Fig. 9. (a) TGA thermographs and (b) decomposition temperature and char yield of PA/PBZ f-IPNs incorporating 100, 80, 60, 50, 40, 20, and 0% BA-m.

Table 4
Surface element compositions of 100% BA-m PA/PBZ f-IPNs, determined by ESCA

Method[a]	C	N	O	Plasma treatment[c]	Heat treatment	
	(mol %)	(mol %)	(mol %)	Time (min)	Temperature (°C)	Time (h)
A[b]	84.01	8.00	7.99			
B	87.90	N.A.	12.01	–	–	–
C	65.26	N.A.	34.73	–	180	1
D	68.54	N.A.	31.45	–	180	4
E	61.71	N.A.	38.02	–	210	2
F	86.68	3.98	9.99	15	–	–
G	82.24	4.43	13.34	15	210	1

[a] Pretreated by spin-coating a BA-m solution (2 mL, 10 wt%, in THF) onto a wafer and baking at 60 °C for 20 min.
[b] Theoretical values.
[c] Performed by Chen et al. [63].

Table 5
Surface free energy parameters of PA/PBZ f-IPNs

Entry	Contact angle (°)			Surface free energy (mJ/m^2)				
	H_2O	DIM	EG	γ_S^{LW}	γ_S^{+}	γ_S^{-}	γ_S^{AB}	γ_S
0% BA-m	102.3	55.7	74.9	31.1	0.01	0.36	0.10	31.2
10% BA-m	101.6	57.0	71.9	30.3	0.03	0.26	0.17	30.5
20% BA-m	100.0	59.8	72.5	28.7	0.03	0.68	0.29	29.0
30% BA-m	105.1	60.2	80.2	28.5	0.05	0.38	0.27	28.8
40% BA-m	109.5	62.1	79.0	27.4	0.01	0.01	0.02	27.4
50% BA-m	108.5	61.0	83.4	28.0	0.10	0.12	0.22	28.2
60% BA-m	109.4	63.8	84.6	26.4	0.08	0.12	0.19	26.6
70% BA-m	111.9	63.5	84.9	26.6	0.06	0.00	0.00	26.6
80% BA-m	112.3	63.4	85.2	26.6	0.06	0.00	0.02	26.7
90% BA-m	113.2	64.4	84.8	26.0	0.02	0.04	0.06	26.1
100% BA-m	113.6	67.2	92.0	24.4	0.32	0.10	0.37	24.8

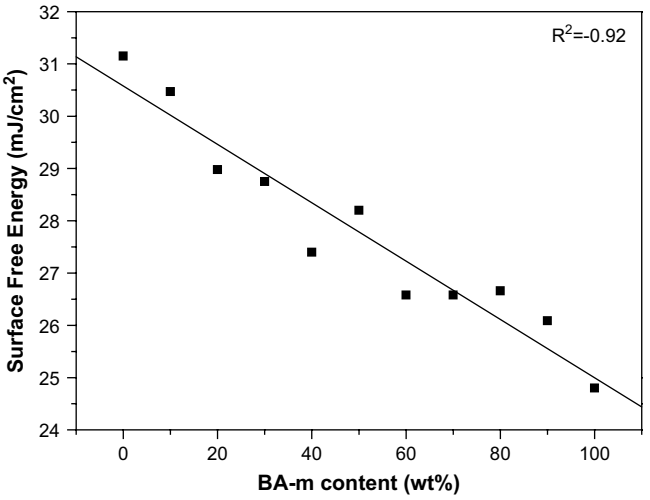

Fig. 10. Linear relationship between the surface free energy and the BA-m content of the PA/PBZ f-IPNs.

4. Conclusion

Because of the presence of strong intramolecular [$O^{-}\cdots HN^{+}$] interactions in pseudo-six-membered rings, most of the ring-opened polybenzoxazine (PBZ) segments folded into stiff helical microdomains that were dispersed in the PA medium. These unique and strong [$O^{-}\cdots HN^{+}$] interactions resulted not only in low miscibility with the PA networks but also hydrophobic surfaces for the PA/PBZ f-IPNs. Through rapid photopolymerization of the PA networks, the phase separation of PBZ was restricted into relatively small sizes (<100 nm). Thus, the thermal and surface properties of PBZ can be adjusted by incorporating it into PA networks. At the optimal composition of 40 wt% BA-m, we obtained transparent (<100 nm PBZ domain size), highly thermostable (5 wt% loss at 316.8 °C), and low-surface-free energy (27.4 mJ/m^2) PA/PBZ f-IPN that we expect would be suitable waterproof coating materials for use in self-cleaning and anti-sticking applications.

References

[1] Coleman MM, Graf JF, Painter PC. Specific interactions and the miscibility of polymer blends. Pennsylvania: Technomic; 1990.
[2] Coleman MM, Painter PC. Prog Polym Sci 1995;20:1–59.
[3] Kuo SW, Chang FC. Macromolecules 2001;34:5224–8.
[4] Kuo SW, Tung P-H, Chang F-C. Macromolecules 2006;39:9388–95.
[5] Sperling LH, Mishra V. Polym Adv Technol 1996;7:197–208.
[6] Krol P, Wojturska J, Statyukha GA, Skladannyy DM. J Appl Polym Sci 2005;97:1855–67.
[7] Roffey C. Photogeneration of reactive species for UV-curing. New York: Wiley; 1997.
[8] Decker C. Prog Polym Sci 1996;21:593–650.
[9] Kharasch MS, Nudenberg W, Mantell GJ. J Org Chem 1951;16:524–32.
[10] Cramer NB, Scott JP, Bowman CN. Macromolecules 2002;35:5361–5.
[11] Bor-Sen C, Saad AK. Macromolecules 1997;30:7322–8.
[12] Li H, Wang X, Song Y, Liu Y, Li Q, Jiang L, et al. Angew Chem Int Ed 2001;40:1743–6.
[13] Aussillous P, Quere D. Nature 2001;411:924–7.
[14] Feng L, Li S, Li Y, Li H, Zhang L, Zhai J, et al. Adv Mater 2002;14:1857–60.
[15] Boutevin B, Pietrasanta Y. Fluorinated acrylates and polyacrylates: derivatives and applications. Paris: EREC; 1988.
[16] Ryntz RA. Prog Org Coat 1994;25:73–83.
[17] Król P, Król B. J Eur Ceram Soc 2006;26:2241–8.
[18] Wu S. Polymer interface and adhesion. New York: Marcel Dekker; 1982.
[19] Tsibouklis J, Stone M, Thorpe AA, Graham P, Nevell TG, Ewen RJ. Langmuir 1999;15:7076–9.
[20] Lau YW, Burns CM. J Polym Sci Part B Polym Phys Ed 1974;12:431–9.
[21] Bernett MK, Zisman WA. J Phys Chem 1960;64:1292–4.
[22] Dettre RH, Johnson Jr RE. J Colloid Interface Sci 1966;21:367–77.
[23] Dettre RH, Johnson Jr RE. J Colloid Interface Sci 1969;31:568–9.
[24] Anton D. Adv Mater 1998;10:1197–205.
[25] Kobayashi H, Owen MJ. Trends Polym Sci 1995;3:330–5.
[26] Schmidt DL, Coburn CE, DeKoven BM, Potter GE, Meyers GF, Fischer DA. Nature 1994;368:41–5.
[27] Ghosh NN, Kiskan B, Yagci Y. Prog Polym Sci 2007;32:1344–94.
[28] Nair CPR. Prog Polym Sci 2004;29:401–98.
[29] Ishida H, Allen DJ. J Polym Sci Part B Polym Phys 1996;34:1019–30.
[30] Ishida H, Low HY. Macromolecules 1997;30:1099–106.
[31] Shen SB, Ishida H. J Appl Polym Sci 1996;61:1595–605.
[32] Shen SB, Ishida H. Polym Compos 1996;17:710–9.
[33] Shen SB, Ishida H. J Mater Sci 1996;31:5945–52.
[34] Kim HJ, Brunovska Z, Ishida H. Polymer 1999;40:1815–22.
[35] Wang CF, Su YC, Kuo SW, Huang CF, Sheen YC, Chang FC. Angew Chem Int Ed 2006;45:2248–51.
[36] Wang CF, Chiou S-F, Ko F-H, Chen J-K, Chou C-T, Huang C-F, et al. Langmuir 2007;23:5868–71.
[37] Liao C-S, Wu J-S, Wang C-F, Chang F-C. Macromol Rapid Commun 2008;29:52–6.
[38] Wang C-F, Chiou S-F, Ko F-H, Chou C-T, Lin H-C, Huang C-F, et al. Macromol Rapid Commun 2006;27:333–7.
[39] Russell VM, Koenig JL, Low HY, Ishida H. J Appl Polym Sci 1998;70:1413–25.
[40] Macko JA, Ishida H. Polymer 2001;42:6371–83.
[41] Burke WJ, Bishop JL, Glennie ELM, Bauer WN. J Org Chem 1965;30:3423–7.
[42] Tsuji Y, Toteva MM, Garth HA, Richard JP. J Am Chem Soc 2003;125:15455–65.
[43] Kim HD, Ishida H. Macromol Symp 2003;1995:123–46.
[44] Goward GR, Sebastiani D, Schnell I, Spiess HW, Kim HD, Ishida H. J Am Chem Soc 2003;125:5792–800.
[45] Schnell I, Brown SP, Low HY, Ishida H, Spiess HW. J Am Chem Soc 1998;120:11784–95.
[46] Dunkers J, Zarate EA, Ishida HJ. Phys Chem 1996;100:13514–20.
[47] Gritchlow GW, Litchfield RE, Sutherland I, Grandy DB, Wilson S. Int J Adhes Adhes 2006;26:577–99.
[48] Erbil HY, Demirel AL, Avci Y, Mert O. Science 2003;299:1377–80.
[49] Ishida H, Lee YH. J Polym Sci Part B Polym Phys 2001;39:736–49.
[50] Ishida H, Lee YH. J Appl Polym Sci 2001;81:1021–34.
[51] Fowkes FM, McCarthy DC, Mostafa MA. J Colloid Interface Sci 1980;78:200–6.
[52] Fowkes FM. J Adhes Sci Technol 1987;1:7–27.
[53] Eaton PJ, Graham P, Smith JR, Smart JD, Nevell TG, Tsibouklis J. Langmuir 2000;16:7887–90.
[54] van Oss CJ, Ju L, Chaudhury MK, Good RJ. J Colloid Interface Sci 1989;128:313–9.
[55] Good RJ, van Oss CJ. In: Schrader ME, Loeb G, editors. Modern approaches to wettability: theory and applications. New York: Plenum Press; 1992. p. 1–27.
[56] Ishida H, Rodriguez Y. Polymer 1995;36:3151–8.
[57] Su Y-C, Yei D-R, Chang F-C. J Appl Polym Sci 2005;95:730–7.
[58] Huang J-M, Kuo S-W, Lee Y-J, Chang F-C. J Polym Sci Part B Polym Phys 2007;45:644–53.
[59] Lee Y-J, Kuo S-W, Huang C-F, Chang F-C. Polymer 2006;47:4378–99.
[60] Su Y-C, Chen W-C, Ou K-I, Chang F-C. Polymer 2005;46:3758–66.
[61] Cui Y, Chen Y, Wang X, Tian G, Tang X. Polym Int 2003;52:1246–8.
[62] Hemvichian K, Kim HD, Ishida H. Polym Degrad Stab 2005;87:213–24.
[63] Chen J-K, Lin I-K, Ko F-H, Huang C-F, Chen K-S, Chan C-H, et al. J Polym Sci Part B Polym Phys 2004;42:4063–74.